Photo-induced spatial modulation of THz waves: opportunities and limitations

Akash Kannegulla,[1] Md. Itrat Bin Shams,[2] Lei Liu,[2] and Li-Jing Cheng[1,*]

[1]*School of Electrical Engineering and Computer Science, Oregon State University, Oregon 97330, USA*
[2]*Department of Electrical Engineering, University of Notre Dame, Indiana 46556, USA*
[*]*chengli@eecs.oregonstate.edu*

Abstract: Programmable conductive patterns created by photoexcitation of semiconductor substrates using digital light processing (DLP) provides a versatile approach for spatial and temporal modulation of THz waves. The reconfigurable nature of the technology has great potential in implementing several promising THz applications, such as THz beam steering, THz imaging or THz remote sensing, in a simple, cost-effective manner. In this paper, we provide physical insight about how the semiconducting materials, substrate dimension, optical illumination wavelength and illumination size impact the performance of THz modulation, including modulation depth, modulation speed and spatial resolution. The analysis establishes design guidelines for the development of photo-induced THz modulation technology. Evolved from the theoretical analysis, a new mesa array technology composed by a matrix of sub-THz wavelength structures is introduced to maximize both spatial resolution and modulation depth for THz modulation with low-power photoexcitation by prohibiting the lateral diffusion of photogenerated carriers.

©2015 Optical Society of America

OCIS codes: (130.1750) Components; (040.2235) Far infrared or terahertz; (230.4110) Modulators; (170.6795) Terahertz imaging.

References and links

1. B. B. Hu and M. C. Nuss, "Imaging with terahertz waves," Opt. Lett. **20**(16), 1716–1718 (1995).
2. T. G. Phillips and J. Keene, "Submillimeter astronomy," Proc. IEEE **80**(11), 1662–1678 (1992).
3. A. Markelz, A. Roitberg, and E. J. Heilweil, "Pulsed terahertz spectroscopy of DNA, bovine serum albumin and collagen between 0.1 and 2 THz," Chem. Phys. Lett. **320**(1-2), 42–48 (2000).
4. E. Brown, D. Woolard, A. Samuels, T. Globus, and B. Gelmont, "Remote detection of bioparticles in THz region," IEEE MTT-S Int. Microw. Symp. Dig. **3**, 1591–1594 (2002).
5. C.-Y. Chen, C.-L. Pan, C.-F. Hsieh, Y.-F. Lin, and R.-P. Pan, "Liquid-crystal-based terahertz tunable Lyot filter," Appl. Phys. Lett. **88**(10), 101107 (2006).
6. B. Sensale-Rodriguez, R. Yan, M. M. Kelly, T. Fang, K. Tahy, W. S. Hwang, D. Jena, L. Liu, and H. G. Xing, "Broadband graphene terahertz modulators enabled by intraband transitions," Nat. Commun. **3**, 780–787 (2012).
7. B. Sensale-Rodriguez, S. Rafique, R. Yan, M. Zhu, V. Protasenko, D. Jena, L. Liu, and H. G. Xing, "Terahertz imaging employing graphene modulator arrays," Opt. Express **21**(2), 2324–2330 (2013).
8. J. Wu, B. Jin, Y. Xue, C. Zhang, H. Dai, L. Zhang, C. Cao, L. Kang, W. Xu, J. Chen, and P. Wu, "Tuning of superconducting niobium nitride terahertz metamaterials," Opt. Express **19**(13), 12021–12026 (2011).
9. Q. Y. Wen, W. Tian, Q. Mao, Z. Chen, W.-W. Liu, Q.-H. Yang, M. Sanderson, and H.-W. Zhang, "Graphene based all-optical spatial terahertz modulator," Sci. Rep. **4**, 7409 (2014).
10. M. Rahm, J. Li, and W. Padilla, "THz wave modulators: a brief review on different modulation techniques," J. Infrared Millim. Terahertz Waves **34**(1), 1–27 (2013).
11. L.-J. Cheng and L. Liu, "Optical modulation of continuous THz waves: towards reconfigurable quasi-optical THz components," Opt. Express **21**(23), 28657–28667 (2013).
12. A. Kannegulla, Z. Jiang, S. Rahman, I. Shams, P. Fay, H. G. Xing, L.-J. Cheng, and L. Liu, "Coded-aperture imaging using photo-induced reconfigurable aperture arrays for mapping terahertz beams," IEEE Trans. Terahertz Sci. Technol. **4**(3), 321–327 (2014).
13. M. I. B. Shams, Z. Jiang, J. Qayyum, S. Rahman, P. Fay, and L. Liu, "A terahertz reconfigurable photo-induced Fresnel-zone-plate antenna for dynamic two-dimensional beam steering and forming," in *IEEE MTT-S International Microwave Symposium* (IEEE, 2015), pp. 1–4.
14. G. Georgiou, H. K. Tyagi, P. Mulder, G. J. Bauhuis, J. J. Schermer, and J. G. Rivas, "Photo-generated THz antennas," Sci. Rep. **4**, 3584 (2014).
15. M. Born and E. Wolf, *Principles of Optics* (Cambridge University, 1999).

#250139 Received 14 Sep 2015; revised 25 Nov 2015; accepted 26 Nov 2015; published 4 Dec 2015
© 2015 OSA

16. L. Liu, Q. Xiao, H. Xu, J. C. Schultz, A. W. Lichtenberger, and R. M. Weikle, "Design, fabrication and characterization of a submillimeter-wave niobium HEB mixer imaging array based on the 'reversed-microscope' concept," IEEE Trans. Appl. Supercond. **17**(2), 407–411 (2007).
17. D. J. Benford, J. W. Kooi, and E. Serabyn, "Spectroscopic measurements of optical components around 1 terahertz," in *Proceedings of Ninth International Symposium of Space Terahertz Technology* (1998), pp. 405–413.
18. E. D. Palik, *Handbook of Optical Constants of Solids* (Academia, 1988).
19. R. Ulbricht, E. Hendry, J. Shan, T. F. Heinz, and M. Bonn, "Carrier dynamics in semiconductors studied with time-resolved terahertz spectroscopy," Rev. Mod. Phys. **83**(2), 543–586 (2011).
20. S. M. Sze, *Physics of Semiconductor Devices* (Wiley Publishers, 1981).

1. Introduction

Over the last decade, the terahertz region (300 GHz - 3000 GHz) of electromagnetic spectrum has become increasingly important in radio astronomy, spectroscopy, medical imaging and defense [1–4]. THz wave modulation as one of the key technologies in THz communication and THz coded aperture imaging has been realized by several approaches [5–8]; however, most of them require prepatterned metal electrodes for the control of pixel matrix, limiting the feasibility and versatility of the technology. In recent years, several methods have been demonstrated to advance the technology for THz wave modulation [9, 10]. Among them, THz modulation through photo-induced carriers on a semiconductor using Digital Light Processing (DLP) projector is considered as a high-performance, reconfigurable and cost-effective approach [11, 12]. This technique takes the advantages of optically generated conductive patterns on semiconductor substrates (e.g., silicon) to manipulate the transmission of THz waves, allowing one to perform a variety of reconfigurable functions, including THz beam steering [13], polarization, focusing and THz resonators. In spite of the success in the experimental demonstration of this technique, the modulation performance was found to be limited by plenty of factors, including the operating conditions and the choice of materials, which were not examined in the prior works. These factors significantly affect the resultant THz modulation and need to be elucidated. To identify the limits and the design rules for optimizing the performance of this approach, we investigate a spectrum of physical parameters that govern the modulation properties, including concentration of photo-excited carriers, carrier lifetime and diffusion property of the carriers in different substrate materials.

In this paper, we theoretically analyze THz wave transmission through intrinsic semiconductor substrates under illumination of visible light patterns. The device performance assessed by its modulation depth, transient modulation response and spatial resolution under various optical illumination conditions and using different substrates materials are investigated. Carrier lifetime of the semiconductor substrate was found to be the key parameter that determines the performance of THz modulation. Intrinsic silicon and germanium have longer carrier lifetime (0.1 – 1 ms) allowing generation of high-concentration excess carrier for THz modulation under low-power continuous-wave (steady-state) photoexcitation, whereas gallium arsenide with a much shorter carrier lifetime (10 – 100 ps) requires high-power pulsed laser excitation to achieve a similar results [14]. In addition, we investigate the impact of optical illumination wavelength, exposure size and substrate dimension on THz wave modulation. The theoretical studies lead to a new design named *mesa-array* structure that utilizes a matrix of sub-THz wavelength structures to restrict lateral diffusion of carriers in semiconductor substrates, remarkably improving both spatial resolution of the photo-induced conductive patterns and the modulation depth of THz waves. The new concept is expected to significantly improve the performance of THz wave spatial modulation using low-power optical excitation.

2. Theory

THz transmission through an optically illuminated semiconductor substrate is calculated by considering a normally incident THz wave penetrating through a multilayer structure as depicted in Fig. 1. The semiconductor substrate situated in the air (refractive index n_0) has a thickness of h and a complex refractive index of $\tilde{n}(x,z)$ at the frequency of the incident THz

#250139 Received 14 Sep 2015; revised 25 Nov 2015; accepted 26 Nov 2015; published 4 Dec 2015
© 2015 OSA

wave. The complex refractive index $\tilde{n}(x,z)$ is determined by the carrier concentration profile generated by a photopattern and can be obtained by solving a continuity equation which yields carrier concentration distributions, and a Lorentz-Drude model which relates the carrier concentration to a frequency-dependent complex dielectric permittivity. One-dimensional and two-dimensional analytical solutions were derived to investigate the effect of illumination aperture size on modulation performance. Three-dimensional carrier distributions are numerically solved using a commercial software package, Lumerical Device, to evaluate the spatial resolution of the THz modulation in different device geometries. A time-dependent solution was deduced to study the transient response of the THz modulation. The THz transmission through a given complex refractive index profile is then calculated using a Fresnel matrix transfer method [15]. As illustrated in Fig. 1(c), the method treats a continuously varying refractive index profile $\tilde{n}(x_i,z)$ over the substrate depth at a particular position x_i as a combination of multiple thin layers each of which has a thickness of δ and a constant refractive index. The transmission analysis offers a whole spectrum of study including, the choice of semiconductor materials, the effect of substrate thickness, optical wavelength for photoexcitation, illumination aperture, THz wave and transient response.

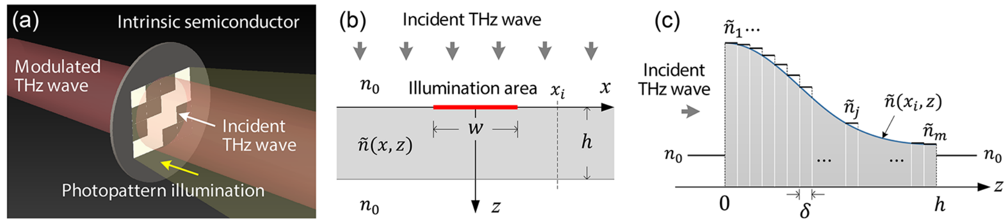

Fig. 1. (a) Setup for photo-induced THz modulation. (b) Schematic diagram for device modeling. (c) Schematic representation of the discretized refractive index profile used in the calculation of THz transmission by a Fresnel transfer matrix method.

Undoped semiconductors, such as intrinsic Si, Ge and GaAs, are transparent to THz waves with a low insertion loss [16, 17]. When a semiconductor surface is illuminated, a region of electron plasma is formed, thus enabling interaction with THz waves. During optical illumination, the absorption of photons creates electron-hole pairs in the semiconductor substrate with a generation rate G and a carrier lifetime τ_e. The carrier generation rate decays exponentially in z-direction and can be expressed as $g(z) = \alpha P_0 (1\text{-}R) e^{-\alpha z}/\hbar\omega$, where α is the absorption coefficient of the substrate at the optical illumination wavelength; P_0 and $\hbar\omega = \hbar\ 2\pi c/\lambda_{ex}$ are the power density and photon energy of the optical illumination at an optical wavelength λ_{ex}, respectively. The reflectivity of the semiconductor substrate is given by $R = |(1-\tilde{n}_S)/(1+\tilde{n}_S)|^2$ using the complex refractive index of the substrate $\tilde{n}_S = n_S + i\kappa_S$ which is a function of the illuminated optical wavelength [18]. The absorption coefficient α is determined by the imaginary part of the substrate refractive index κ_s at the illumination wavelength λ_{ex}, *i.e.*, $\alpha = 4\pi\ \kappa_s/\lambda_{ex}$. .

The photoexcited carrier concentration profile $N_e(x,z,t)$ in the semiconductor substrate is given by the solution to a continuity equation:

$$\frac{\partial N_e}{\partial t} = D_{eff}\nabla^2 N_e - \frac{N_e}{\tau_e} + g. \qquad (1)$$

with the operator $\nabla^2 = \frac{\partial^2}{\partial x^2} + \frac{\partial^2}{\partial z^2}$ for a two-dimensional Cartesian coordinate system. The physical property of the substrate material is determined by carrier lifetime τ_e and effective carrier diffusion coefficient $D_{eff} = 2\mu_{eff}\ k_B T/q$ contributed by both electrons and holes in a form of a combined effective carrier mobility $\mu_{eff} = (1/\mu_e + 1/\mu_h)^{-1}$. The carriers are generated by the absorption of light in the area with a width of w and then diffuse over the

semiconductor substrate with a thickness of h situated between two layers of air with infinite thicknesses. We assume that a negligible surface recombination on both top and bottom surfaces of the substrate which gives the boundary conditions at $z = 0$ and $z = h$ prescribed as $\partial_z n(x,z)\big|_{z=0} = 0$ and $\partial_z n(x,z)\big|_{z=h} = 0$, respectively. The steady-state solution satisfying the partial differential equation and the boundary conditions is

$$N_e^{2D}(x,z) = \int_0^h \int_{-w/2}^{w/2} \frac{g(\eta)}{D_{eff}} G(x,z,\xi,\eta)\, d\xi\, d\eta. \tag{2}$$

with the Green's function $G(x,z,\xi,\eta)$ defined by

$$\begin{aligned} G(x,z,\xi,\eta) = \frac{1}{2\pi}\sum_{n=-\infty}^{\infty}\Big[& K_0\left(\sqrt{(x-\xi)^2 + [z-(2nh+\eta)]^2}\Big/L_D\right) \\ & + K_0\left(\sqrt{(x-\xi)^2 + [z-(2nh-\eta)]^2}\Big/L_D\right)\Big]. \end{aligned} \tag{3}$$

where g is the carrier generation rate described previously, and K_0 in the Green's function, $G(x,z,\xi,\eta)$, is the modified Bessel function of the second kind of integer order 0 and is a function of carrier diffusion length $L_D = (D_{eff}\,\tau_e)^{1/2}$. At a flood exposure condition, *i.e., $w \to \infty$*, the system reduces to a one-dimensional problem, yielding a solution of

$$N_e^{1D}(z) = \frac{\tau_e \alpha P_o}{\hbar\omega}\frac{1-R}{1-(\alpha L_D)^2}\left[e^{-\alpha z} - \alpha L_D\left(e^{\frac{-z}{L_D}}\left(\frac{1-e^{-(\alpha+1/L_D)h}}{1-e^{-2h/L_D}}\right) - e^{\frac{z}{L_D}}\left(\frac{1-e^{-(\alpha-1/L_D)h}}{1-e^{2h/L_D}}\right)\right)\right]. \tag{4}$$

For the material with small carrier lifetime and therefore a much shorter diffusion length comparing with the substrate thickness, *i.e.,* $L_D << h$, Eq. (4) reduces to

$$N_e^{1D}(z)\Big|_{L_D \ll h} = \frac{\tau_e \alpha P_o (1-R)}{\hbar\omega}\frac{1}{1-(\alpha L_D)^2}\left(e^{-\alpha z} - \alpha L_D e^{-z/L_D}\right). \tag{5}$$

To study the transient response of THz modulation, a time-dependent 1D carrier concentration profile responding to a periodic pulsed illumination was deduced from Eq. (1). The continuous periodic pulse with a period T_p is generated by using a pulse wave function $S_T(t)$ defined by

$$S_T(t) = \frac{1}{2} + \sum_{n=1}^{\infty}\frac{2}{n\pi}\sin\left(\frac{\pi n}{2}\right)\cos\left(\frac{2\pi n}{T_p}t\right). \tag{6}$$

The transient carrier concentration is given by

$$N_e^{1D-t}(z,t) = \int_0^t \int_0^h g(\eta) S_T(\tau) G_t(z,\eta,t-\tau)\, d\eta\, d\tau. \tag{7}$$

with the Green's function $G_t(z,\eta,t)$ defined by

$$G_t(z,\eta,t) = e^{-t/\tau_e}\left[\frac{1}{h} + \frac{2}{h}\sum_{n=1}^{\infty}\cos\left(\frac{n\pi z}{h}\right)\cos\left(\frac{n\pi\eta}{h}\right)e^{-D_{eff}\left(\frac{n\pi}{h}\right)^2 t}\right]. \tag{8}$$

The total carrier concentration N_s, which sums up the photo-excited carrier concentration N_e^X (X = 2D, 1D or 1D-t) and the intrinsic carrier concentration N_i, *i.e.,* $N_s = N_e^X + N_i$, is then exploited to determine the corresponding frequency-dependent complex dielectric constant $\tilde{\varepsilon}_D = \varepsilon_{re} + i\varepsilon_{im}$ throughout the substrate using a Lorentz-Drude model as [19],

#250139 Received 14 Sep 2015; revised 25 Nov 2015; accepted 26 Nov 2015; published 4 Dec 2015
© 2015 OSA

$$\varepsilon_{re}(x,z,\omega) = -\frac{N_s q^2 \omega^2}{m_e(\omega^4 + \omega^2\gamma_e^2)\varepsilon_0} - \frac{N_s q^2 \omega^2}{m_h(\omega^4 + \omega^2\gamma_h^2)\varepsilon_0} + \varepsilon_\infty.$$
$$\varepsilon_{im}(x,z,\omega) = \frac{N_s q^2 \omega\gamma_e}{m_e(\omega^4 + \omega^2\gamma_e^2)\varepsilon_0} + \frac{N_s q^2 \omega\gamma_h}{m_h(\omega^4 + \omega^2\gamma_h^2)\varepsilon_0}. \tag{9}$$

Where, ω is the frequency of THz radiation, ε_∞ the dielectric constant of the material, ε_0 the permittivity of vacuum, m_e and m_h the effective masses of electron and hole, respectively. The electron and hole damping coefficients, γ_e and γ_h, are calculated by the inverse of the average electron or hole collision time depending on the effective mass $m_{e,h}$ and the mobility $\mu_{e,h}$ of carriers, *i.e.,* $\gamma_{e,h} = (m_{e,h}\ \mu_{e,h}/q)^{-1}$. Further, the complex refractive index of the photoexcited semiconductor substrate, $\tilde{n} = n_1 + i\kappa_1$ at the THz frequency range can be calculated using complex dielectric constant and is given by

$$n_1(x,z,\omega) = \sqrt{\left(\varepsilon_{re} + \sqrt{\varepsilon_{re}^2 + \varepsilon_{im}^2}\right)/2}.$$
$$\kappa_1(x,z,\omega) = \sqrt{\left(-\varepsilon_{re} + \sqrt{\varepsilon_{re}^2 + \varepsilon_{im}^2}\right)/2}. \tag{10}$$

The transmission of a normally incident THz wave through the substrate is calculated by using a Fresnel transfer matrix technique to take care of the graded refractive index in the substrate induced by photoexcitation. The graded refractive index is considered as a multilayer structure composed by m multiple isotropic and homogeneous thin, parallel layers with the same thickness of δ and a complex refractive index of $\tilde{n}_j = \tilde{n}(z = jh/m)$ for the jth layer. For the device structure studied here, $\tilde{n}_0$ and $\tilde{n}_m$ are equal and are the refractive index of the air. The thickness δ is chosen to be 1 μm which is much smaller than diffusion length and THz wavelength to insure the accuracy of the results. The transmission can be obtained from a 2 × 2 scattering matrix

$$\mathbf{S} = \begin{pmatrix} S_{11} & S_{12} \\ S_{21} & S_{22} \end{pmatrix} = \mathbf{I}_{01} \prod_{j=1}^{m} \mathbf{L}_j \mathbf{I}_{j(j+1)}. \tag{11}$$

The transfer matrix $\mathbf{I}_{j(j+1)}$ defines the wave propagation at the interface between the jth and (j + 1)th layer and reads

$$\mathbf{I}_{j(j+1)} = \frac{1}{t_{j(j+1)}} \begin{pmatrix} 1 & r_{j(j+1)} \\ r_{j(j+1)} & 1 \end{pmatrix}. \tag{12}$$

where $r_{j(j+1)} = \left(\tilde{n}_{j+1} - \tilde{n}_j\right) \big/ \left(\tilde{n}_{j+1} + \tilde{n}_j\right)$ and $t_{j(j+1)} = 2\tilde{n}_j / (\tilde{n}_{j+1} + \tilde{n}_j)$ are the Fresnel coefficients for a zero-order propagation at the interface j (j + 1). The transfer matrix $\mathbf{L}_j$ is defined as

$$\mathbf{L}_j = \begin{pmatrix} e^{i\phi_j} & 0 \\ 0 & e^{-i\phi_j} \end{pmatrix}. \tag{13}$$

where ϕ_j defined by $\phi_j = 2\pi\delta\tilde{n}_j \big/ \lambda_T$ is the phase shift for a normal incident THz wavelength λ_T passing through the jth layer which has a complex refractive index of $\tilde{n}_j$ and a thickness of δ. From the 2 × 2 scattering matrix **S** it is possible to calculate the transmission of THz wave using

#250139 Received 14 Sep 2015; revised 25 Nov 2015; accepted 26 Nov 2015; published 4 Dec 2015
© 2015 OSA

$$T = \left| \frac{1}{S_{11}} \right|^2 . \tag{14}$$

3. Results and discussion

Optical illumination of semiconductors generates free carriers and lowers the THz transmission through it. Therefore, any physical property that influences the photo-induced free carrier concentration will regulate the performance of THz modulation. In this section, we systematically discuss the physical factors, including substrate thickness, THz frequency, optical illumination width, and optical illumination wavelength, that determine THz modulation based on theoretical calculations described in the previous section. The results provide design guidelines to optimal modulation depth, speed and spatial resolution which are essential to achieve high-performance THz tunable components for advanced sensing and imaging. The semiconductor substrates employed for the study include undoped crystal silicon, germanium, and gallium arsenide. The 590 GHz wave was chosen for investigating THz modulation properties. The physical parameters of the materials used for calculation are tabulated in Table 1.

Table 1. Optical and electrical properties of intrinsic semiconductor substrates [18, 20].

Parameters	Si	Ge	GaAs
n_s and κ_s at λ_{ex} = 550 nm	4.08 / 0.028	5.16 / 2.20	4.31 / 2.21
Absorption coefficient α (cm^{-1}) at λ_{ex} = 550 nm	6.70×10^3	5.03×10^5	5.05×10^5
Generation rate g (cm^{-3}s^{-1}) at λ_{ex} = 550 nm	1.64×10^{22}	6.70×10^{23}	1.11×10^{23}
Diffusion coefficient D_{eff} (cm^2/s)	17.31	63.88	19.10
Effective carrier lifetime τ_e (s)	10^{-4}	10^{-3}	10^{-8}
Diffusion length L_D (cm)	0.0416	0.2527	0.00044
Electron Mobility μ_e (cm^2/Vs)	1500	3900	8500
Hole Mobility μ_h (cm^2/Vs)	450	1900	400
Intrinsic carrier concentration N_i (cm^{-3})	1.45×10^{10}	2.40×10^{13}	1.79×10^6
Electron effective mass m_e	0.26 m_o	0.12 m_o	0.067 m_o
Hole effective mass m_h	0.38 m_o	0.21 m_o	0.39 m_o
Dielectric constant ε_∞	11.7	16.2	13.1

3.1 Effect of substrate material and thickness

Figure 2 shows a series of 590 GHz transmission spectra and modulation depths for different substrate materials as functions of thickness under illumination of 550 nm light and multiple power densities. Without optical illumination, the THz transmissions through all the three substrate materials vary periodically between 0.2 or 0.3 and ~1 with the increase of the substrate thickness as the result of the interference of THz waves in the dielectric materials (*i.e.*, standing wave effect). The transmission peaks for Ge substrate decay gradually with thickness due to a non-negligible absorption at 590 GHz. As illuminated with 1 W/cm^2 optical power density, the THz waves through Si and Ge substrates are significantly attenuated, resulting in a modulation depth ranging from −15 to −25 dB for Si and that from −100 to −300 dB for Ge. A high modulation depth is observed in Ge substrate and a 0.1 W/cm^2 optical illumination is sufficient to achieve a modulation depth of −20 to −30 dB. Despite the difference in the magnitude, the modulation depths in Si and Ge increase with substrate thickness. On the contrary, GaAs exhibits almost no THz modulation under the given photoexcitation power density of 1 W/cm^2.

The effect of substrate material and substrate thickness on the corresponding THz modulation, except for the interference phenomenon, can be explained by the photo-excited carrier concentration profiles summarized in Fig. 3. For the illuminated Si and Ge substrates, thinner substrates are found to cumulate more carriers because of the limited space available for carriers to diffuse and recombine. When the substrate becomes much thicker than the diffusion length ($h >> L_D$), the excess carrier concentration is much lower and follows an

#250139 Received 14 Sep 2015; revised 25 Nov 2015; accepted 26 Nov 2015; published 4 Dec 2015
© 2015 OSA

exponential decay across the substrate. A thinner substrate gives more photoexcited carriers but exhibits weaker THz modulation depth, especially when it becomes thinner than the attenuation distance of THz waves which is in the order of the THz wavelength. A thicker substrate providing less excess carrier concentration, however, offers longer distance for efficient attenuation of THz wave. Large photogenerated carrier concentration and high modulation depth observed in Ge substrate are the results of the greater optical absorption coefficient at 550-nm wavelength, larger diffusion coefficient and longer carrier lifetime in Ge. Although GaAs has a high absorption coefficient for 550 nm light as well, the short carrier lifetime (10^{-8} s) leads to a low carrier concentration level (about 3 to 4 orders of magnitude lower than that of Si or Ge) under the same illumination power density and a steep exponential decay of carrier concentration within 100 μm. The small diffusion length ($h >> L_D$) in GaAs makes the carrier concentration profile almost independent to the substrate thickness. To employ GaAs substrate for THz modulation, a high-power photoexcitation is required to generate sufficient excess carriers. A pulsed laser that delivers a few μJ/cm^2 energy in a 100 fs pulse duration with a period of picoseconds can equivalently produce a constantly high power density in the order of kW/cm^2 to MW/cm^2 to generate carriers satisfactory to THz modulation [13]. The large minority carrier lifetime in Si and Ge substrates allows generation of high carrier concentration with low-power photo-excitation, enabling the use of cost-effective light sources for THz modulation. It is noteworthy that in practice the carrier lifetime could be dominated by the defect density in the bulk or on the surface of the substrate resulting in a lower modulation depth.

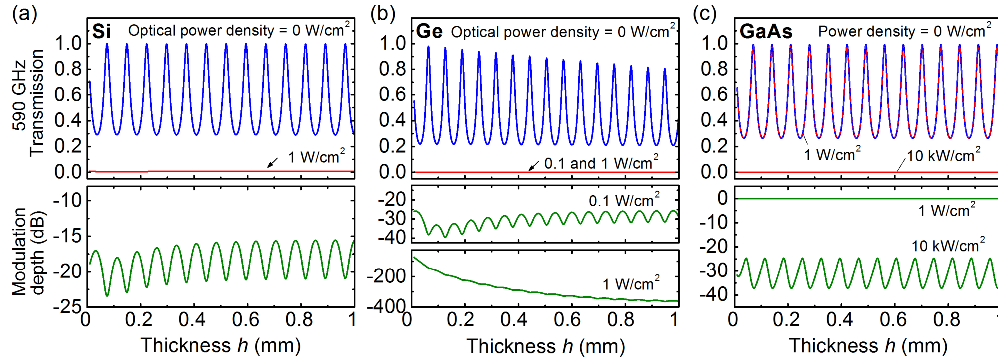

Fig. 2. Transmission and modulation depth of (a) Si, (b) Ge, and (c) GaAs substrates as functions of substrate thickness h up to 1 mm under illumination of continuous 550-nm light waves at various power densities.

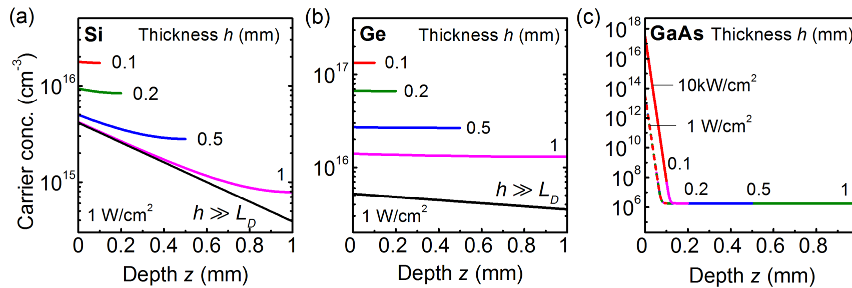

Fig. 3. Carrier concentration profiles in (a) Si, (b) Ge and (c) GaAs substrates with various thicknesses illuminated by continuous 550-nm light waves at a power density of 1 W/cm^2. An equivalent 10kW/cm^2 continuous wave illumination is applied for GaAs substrate.

A proper substrate thickness is required for efficient modulation at a specific THz wave frequency as a consequence of the interference of THz wave in the substrate. On the basis of the above analysis, for better comparison in the following studies on the modulation of 590

GHz wave, we choose the substrate thicknesses to be 450 μm for Si, 440 μm for Ge and 420 μm for GaAs (see Fig. 2) to establish maximal modulation depths for 590 GHz waves in all these materials. A 1 W/cm^2 light source is used to evaluate the performance of THz modulation in Si and Ge substrates, while a much larger optical power density of 10kW/cm^2 is used for GaAs substrate.

3.2 Effect of THz frequency

THz transmission spectra and modulation depths for Si and Ge substrates are analyzed over the THz wave frequency ranging from 10 GHz to 10 THz as shown in Fig. 4. This analysis was performed at various optical power densities of 0, 0.1, 0.2, 0.5 and 1 W/cm^2 for 450-μm-thick Si, whereas the same analyses are performed using optical power densities of 0, 0.01, 0.02, 0.05, 0.1 and 1 W/cm^2 for 440-μm-thick Ge, and 0, 1, 2, 5, and 10 kW/cm^2 for 420-μm-thick GaAs. The results show that the transmission of THz radiation reduces as the optical power density increases, due to the enhanced photoconductivity.

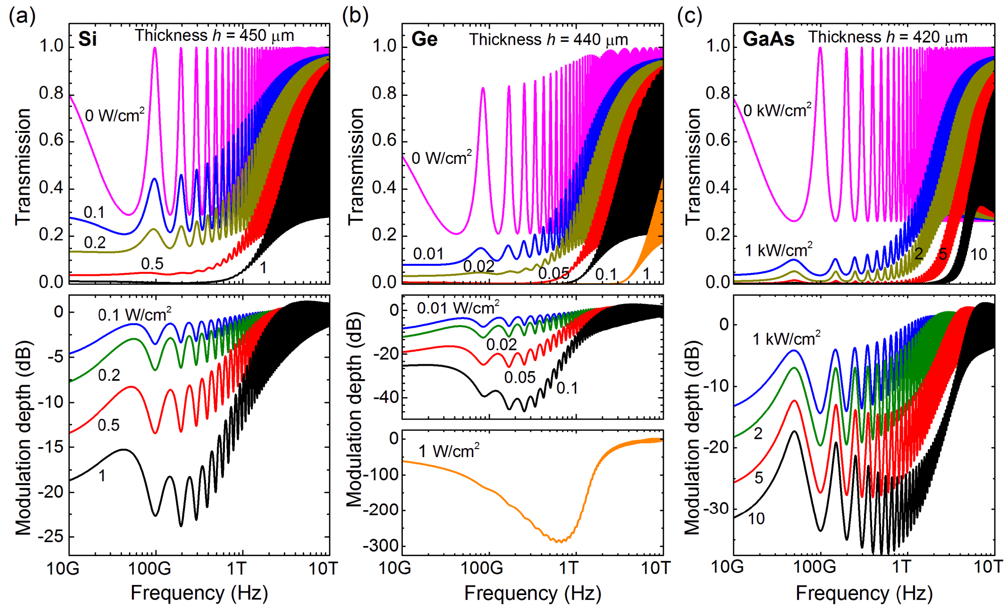

Fig. 4. Transmission spectra and modulation depth spectra of Si (a), Ge (b), and GaAs (c) substrates at THz range under various optical illumination power densities.

Oscillation in transmission was observed for all the materials as the incident THz wave frequency varies. A relatively high modulation depth is observed with Ge comparing with Si at the same optical power densities because of high photogeneration of carriers in Ge. For example, Si shows a modulation depth of about −3 dB at 0.1 W/cm^2 optical power density, whereas Ge reaches a −30 dB modulation depth. An exceptionally high modulation depth of Ge over Si makes it more desirable for THz modulators. It can be seen that the modulation capability becomes weaker as the incident THz wave frequency approaches as high as 10 THz and as low as 10 GHz. The upper frequency limitation for effective modulation is determined by the plasma frequency of the photo-excited semiconductor, *i.e.,* $\omega_p = (N_s e^2/\varepsilon_0 m^*)^{1/2}$. Being able to effectively attenuate an incident THz wave requires the plasma frequency of the substrate greater than the incident THz wave frequency. Therefore, a large optical power density is necessary to boost adequate carrier concentration N_s for high frequency THz modulation. The plasma frequencies of Si and Ge substrate under the same 550 nm, 1 W/cm^2 illumination are calculated to be 1.2 THz and 4.5 THz, respectively. These explain why the THz modulation becomes less efficient as the THz frequencies are beyond these values. The plasma frequency for GaAs substrate illuminated at 550 nm 10 kW/cm^2 is about 19 THz,

larger than the upper frequency limit for modulation, *i.e.*, about 2 THz indicated in Fig. 4(c). The overestimation may be attributed to the fact that the THz waves are modulated by only a few micrometer thick high-concentration photo-excited carriers near the surface of GaAs substrate rather than a bulk material which is considered in the calculation of the plasma frequency. On the other side, the lower frequency limitation results from the fact that the substrate becomes comparable to or even shorter than the incident THz wavelength and turns out to be less efficient in attenuating the long THz waves. A small positive modulation depth is observed in GaAs substrate with the THz frequency close to 10 THz. It is because a thin layer of photo-generated carriers formed on the surface functions as an anti-reflective coating increasing the transmission of THz waves.

3.3 Effect of optical illumination wavelength

The wavelength of optical illumination determines the carrier generation rate g and, thus, the resulting THz modulation depth. Figure 5 shows the transmission spectra and modulation depths for the penetration of 590 GHz wave through the three types of substrates as a function of illuminated optical wavelength with multiple power densities. The THz modulation depth for both substrates increases with illumination wavelength. The trend is mainly attributed to the fact that a longer optical wavelength λ_{ex} yields a thicker absorption and hence a higher photogenerated carrier concentration in the substrates. Calculation based on the experimental refractive index data obtained from [18] suggests that with the increase of optical wavelength both optical absorption coefficient α and refractivity R of the substrates decrease (α has a stronger effect), overall resulting in the lowering of the carrier generation rate g. Despite the smaller generation rate, the long-wavelength light penetrates further into the substrate (*i.e.*, $1/\alpha$ increases) and excites the carriers over a thicker volume leading to a resultant higher carrier concentration. This effect of absorption depth becomes dominant and overcomes the reduction of generation rate at a longer optical wavelength. For GaAs substrate, the effect of optical illumination wavelength will be much stronger with λ_{ex} > 800 nm in which the absorption coefficient drops dramatically. The result is not shown here. In general, a higher modulation depth of THz waves can be achieved by using a longer optical wavelength for photo-excitation. A 550-nm optical illumination is chosen for all the analyses in this article because the Digital Light Processing (DLP) projector used in our prior experimental studies has a peak wavelength of about 550nm [12].

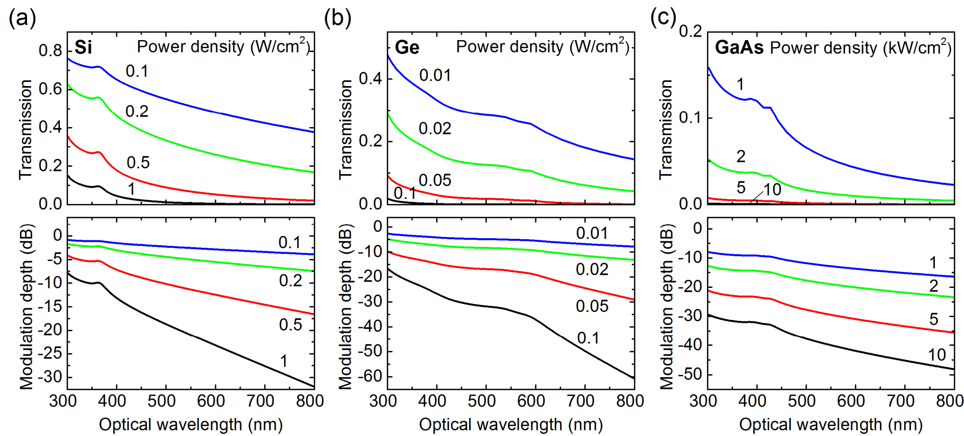

Fig. 5. Transmission and modulation depth of a 590 GHz wave transmitted through 450-μm thick Si (a), 440-μm thick Ge (b) and 420-μm thick GaAs (c) substrates illuminated with various optical wavelengths and power densities.

#250139 Received 14 Sep 2015; revised 25 Nov 2015; accepted 26 Nov 2015; published 4 Dec 2015

© 2015 OSA

3.4 Effect of substrate material on THz modulation speed

As one of the key performance specifications in THz imaging, modulation speed of THz waves determines the highest achievable frame rate of coded aperture imaging as described in our previous work [12]. Figure 6(a) shows the time-dependent transmission and modulation depth of 590 GHz wave through Si, Ge and GaAs substrates in response to optical illumination pulses with a 20-fold carrier lifetime pulse period (i.e., 20 τ_e) and 50% duty cycle. The optical illumination power densities are 1 W/cm^2 for Si and Ge, and 10 kW/cm^2 for GaAs. The timescale is normalized to the carrier lifetime τ_e of each material which are 0.1 ms for Si, 1 ms for Ge, and 10 ns for GaAs, respectively. We define the time taken to modulate THz wave from 90% to 10% transmission as transfer time and the time taken to return from 10% to 90% transmission as recovery time. Figure 6(b)-6(d) show the time-dependent carrier concentration profiles across the substrates, during illumination (t = 0 to 10 τ_e) and recovery (t = 10 to 20 τ_e). The transfer time and recovery time are proportional to the carrier lifetime τ_e of the material. For each of the three materials, it takes about 1 τ_e of illumination to reach a saturate concentration; after the illumination ceases, it takes the entire 10 τ_e recovery cycle for the concentration to gradually return to the initial value. A recovery cycle of 10 τ_e is long enough for Si and Ge to regain their intrinsic carrier concentrations. The same duration allows GaAs to recover the carrier concentration down to 10^{12} cm^{-3}, low enough to make it transparent to THz waves. While the excess carrier concentrations distribute over the entire Si and Ge substrates responding to the illumination pulses, the generation of carrier concentration in GaAs substrate only occurs nearby the surface.

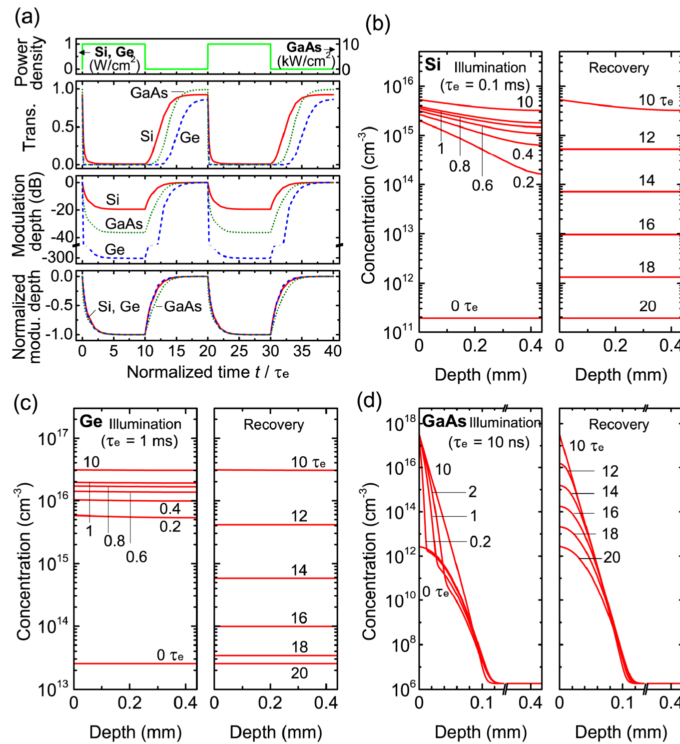

Fig. 6. (a) Temporal modulation of 590 GHz wave through Si, Ge and GaAs substrate using a pulsed optical illumination with a period of 20-fold carrier lifetime (20 τ_e) for each material. Transient response of carrier concentrations in 450 µm thick Si (a), 440 µm thick Ge (b) and 420 µm thick GaAs (c). Carrier concentration rises upon illumination at time t = 0-10 τ_e, and recovers after light is off from t = 10 to 20 τ_e. The carrier lifetimes τ_e used for calculation are 0.1 ms for Si, 1 ms for Ge, and 10 ns for GaAs.

#250139 Received 14 Sep 2015; revised 25 Nov 2015; accepted 26 Nov 2015; published 4 Dec 2015
© 2015 OSA

The carrier lifetime τ_e of Si is 10 times less than that of Ge, resulting in a fast modulation response in Si, with a transfer time of 0.06 ms (= 0.6 τ_e) and a recovery time of 0.52 ms (= 5.2 τ_e). GaAs substrate has a transfer time of 1.2 ns (= 0.12 τ_e) and a recovery time of 50 ns (= 5 τ_e). The maximal modulation depths of about −20 dB are found for Si and GaAs substrates during illumination cycles, while Ge substrate can reach down to −170 dB. The greater modulation depth observed in Ge substrate is the result of larger $g\ \tau_e$ product and the increase of carrier concentration over the entire substrate which have been discussed in the previous section. The normalized modulation depth in Fig. 6(a) shows that the Si and Ge substrates have an identical modulation dynamics while GaAs has a faster transfer responses but slower recovery response. The different dynamic responses can be explained from two aspects. First, diffusion length of carrier in GaAs is much shorter than the substrate thickness, *i.e.,* $D_{eff}\,\tau_e\,/h^2 << 1$. As the result, the geometrical effect which is also indicated as the second term of Eq. (8) becomes less important, leading to a relative rapid concentration response in GaAs. The fast concertation response is reflected in the rapid transfer time. In addition, because GaAs substrate relies on a thin layer of photo-generated carriers in the vicinity of the surface for THz modulation, a relatively higher concentration is required to produce a comparable modulation depth. This explains why the Si substrate with an excess carrier concentration of 10^{15} cm^{-3} produces a similar modulation depth to the GaAs substrate with a higher excess carrier concentration of 10^{17} cm^{-3}. The high excess carrier concentration in GaAs further explains a longer recovery time for regaining THz transmission.

It is worthwhile to know that the calculated modulation speed for Si substrate is about 10 times faster than the experimental results the authors demonstrated using digital mirror device (DMD) in [11]. The slower modulation speed observed in the DMD-based photo-induced THz modulation is the result of the limited scanning rate across the entire DMD matrix [11].

3.5 Effect of photo-excitation area

The spatial resolution of THz modulation is investigated by examining the carrier concentration distributions over the substrate with various illumination areas. Figure 7 shows the carrier concentration distributions across the substrate surface and the substrate cross-section when the substrate is exposed to a continuous, uniform light beams with the width ranging from 50 to 1000 μm. For Si and Ge substrates, higher carrier concentrations are established in the substrate with the increase of illumination area. The width of the resulting carrier concentration profile is determined by the diffusion length of the excess carriers diffusing from the illuminated area. Although the carrier generation rate, g, is independent of the illumination area, a large-area illumination generates a larger volume of carriers in total which allows to sustain a high concentration level under the effect of lateral diffusion. The diffusion coefficient of the carriers in Ge is greater than that in Si leading to a broader carrier concentration profile and a more drastic drop in carrier concentration with the decrease of illumination area. GaAs, on the other hand, has a much shorter diffusion length; all the photogenerated carriers stay in the illuminated area forming a sharp photoconductive pattern. The depressed lateral diffusion allows to sustain a constant carrier concentration independent of the illumination area. The cross-sectional carrier distributions in Si, Ge and GaAs substrates illuminated by a 100-μm wide light beam are detailed as the 2D concentration profiles in Fig. 7(b). As shown in Fig. 7(c) the lateral diffusion of the photogenerated carriers deteriorates the spatial resolution of THz transmission, especially in the Ge substrate. Moreover, the illumination area significantly affects the resulting THz transmission leading to inconsistent THz modulation depth induced by the photopatterns with all different sizes and shapes. The drawback could depreciate the utility of the modulation technique. The photoconductive pattern generated on GaAs substrate can be highly resolved and produces consistent modulation depths regardless of the illumination size.

#250139 Received 14 Sep 2015; revised 25 Nov 2015; accepted 26 Nov 2015; published 4 Dec 2015
© 2015 OSA

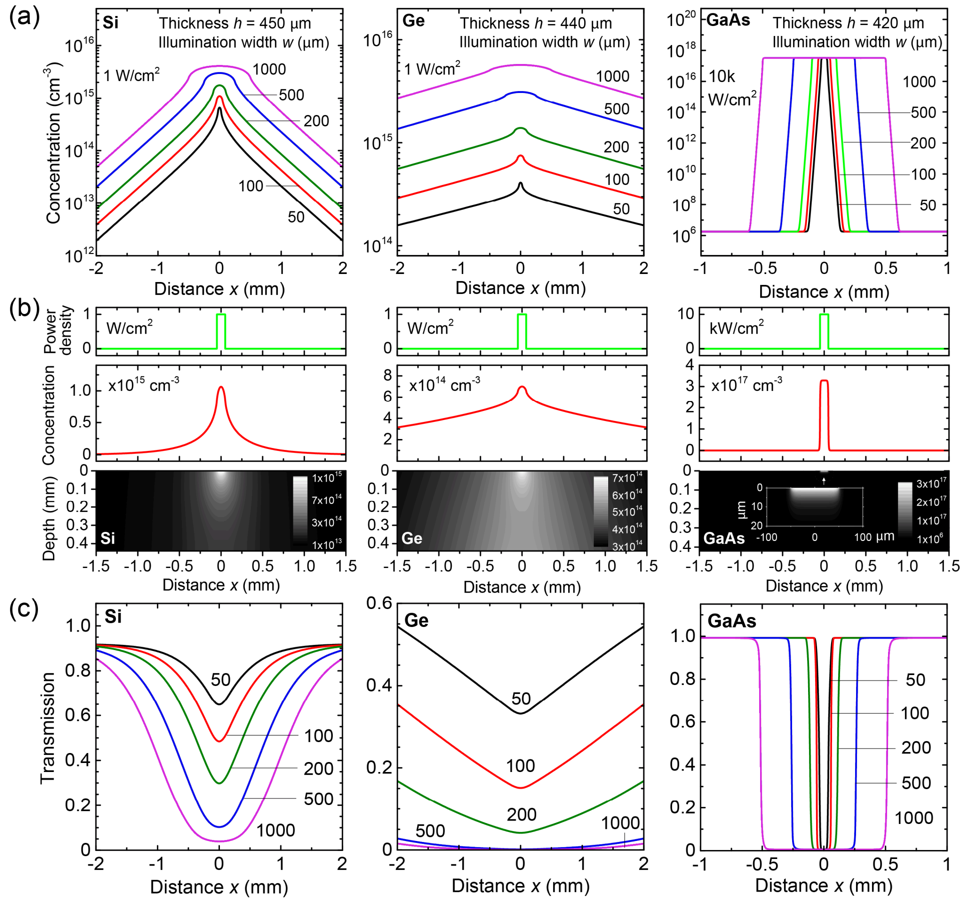

Fig. 7. (a) Carrier concentration profiles over the surface of Si, Ge and GaAs substrates. (b) 2D carrier distribution over the cross-sectional Si and Ge substrates illuminated by a 100-µm wide light beam. (c) Spatial distribution of 590 GHz transmission through Si, Ge and GaAs substrates under illumination of 550-nm, 1 W/cm^2 continuous light waves for Si and Ge, and 10kW/cm^2 for GaAs with various illumination widths in micrometer.

Figure 8 summarizes the carrier concentration, THz transmission, and modulation depth for all these three substrates as functions of optical illumination width ranging from 10 µm to 5 mm. With the illumination width less than 1000 µm, more excess carrier concentration is found in Si than Ge due to slow diffusion of carriers in Si that allows more carriers to be maintained. However, for larger illumination widths (w > 1000 µm), the lateral diffusion becomes less influential to the concentration of the patterns and the effect of carrier generation, *i.e.,* $g\ \tau_e$ product, becomes more dominant. In spite of the discrepancy of excess carrier concentration levels at different illumination widths, Ge always has a greater modulation depth over the whole range of illumination width. The large diffusion length in Ge creates a uniformly high carrier concertation level throughout the entire substrate (see Fig. 7(c) and 7(d)) resulting in more effective THz modulation. GaAs provides a consistent modulation depth despite the illumination size. The results imply that GaAs is more appropriate for THz applications that require photopattern technique such as imaging, filters and polarizers, despite the requirement of much higher photoexcitation power.

#250139 Received 14 Sep 2015; revised 25 Nov 2015; accepted 26 Nov 2015; published 4 Dec 2015
© 2015 OSA

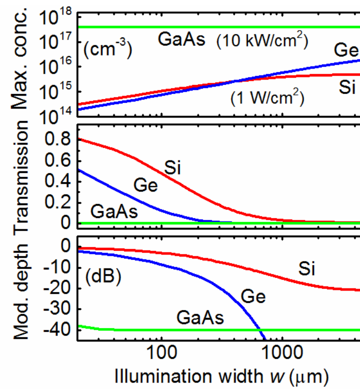

Fig. 8. Maximum concentration of photogenerated carriers, transmission, and modulation depth in Si, Ge and GaAs substrates as functions of illumination width w. Illumination wavelength 550 nm, power density 1 W/cm^2 for Si and Ge, and 10kW/cm^2 for GaAs.

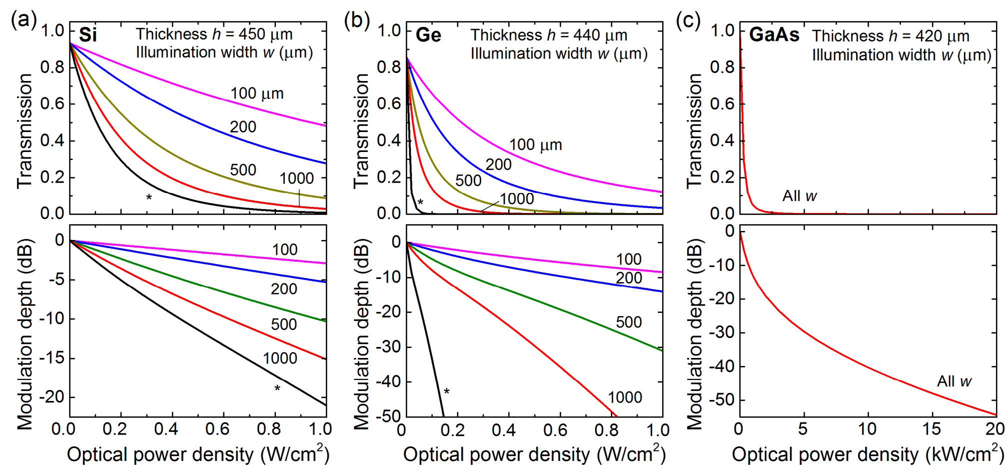

Fig. 9. Transmission and maximal modulation depth of 590 GHz wave through Si (a), Ge (b) and GaAs (c) substrates as functions of illumination power density of 550 nm-light wave with various illumination width w. The asteriated curves represent the results of flat exposure.

The THz transmission and modulation depth shown in Fig. 9 indicate that the performance of THz modulation using Si and Ge substrates strongly depends on the area of illumination. It is necessary to generate photopatterns with sufficiently high optical power density to ensure enough modulation depth for all sizes of photopatterns. Although GaAs substrate exhibits size-independent THz modulation, it requires a much large illumination power density. The rationale implies that if the lateral carrier diffusion observed in Si and Ge can be prohibited, *i.e.*, to force the photogenerated carriers to undergo a 1D diffusion in the vertical direction, it is possible to utilize low-power optical illumination to achieve a modulation depth as high as that under flood exposure (the asteriated curves in Fig. 9), more importantly, independent of illumination size.

3.6 Mesa array technique

The degraded spatial resolution of THz modulation and the illumination-area dependent modulation depth are all the restuls of the lateral diffuion of the photogenerated carriers in the substrate. To overcome the issue, we propose a conceptual solution called mesa array technique to effectively eliminate the lateral diffusion of carriers. The mesa array structure is a matrix of submicron deep trench structure fabricated on a semicodnuctor substrate forming

an array of isolated mesa structures. The dimension of each mesa structure is designed to be much smaller than the THz wavelength and the diffusion length, e.g., a 5 μm by 5 μm square. When such a sub-wavelength and sub-diffusion length structure is illuminated, it confines the photogenerated carriers in the isolated structure, allowing 1D diffusion in the vertical direction.

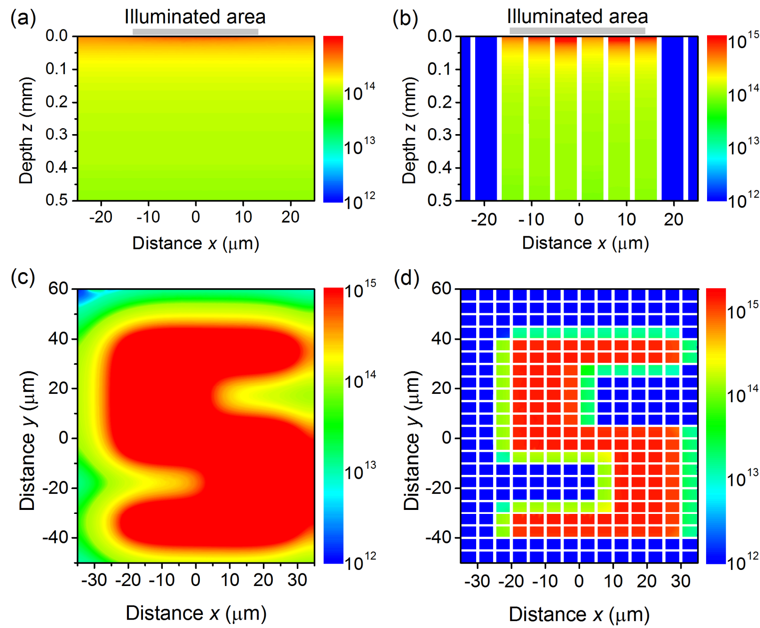

Fig. 10. (a) and (b) Cross-sectional carrier concentration profile over a 500 μm thick bare Si substrate and a mesa array Si substrate 0.01 ms after illuminated by a 25-μm wide light pattern from top. (c) and (d) Carrier concentration over the surface of a 70 μm × 110 μm bare Si substrate and mesa array substrate about 0.02 ms after illuminated a photopattern of alphabete letter "S". Optical wavelength 550 nm; optical power density 1 W/cm^2.

To demonstrate the capability of high spatial resolution realized by the mesa array technique, we compare the carrier concentration profiles photogenerated on a bare Si susbtrate and a Si substrate with the mesa array structure under the illumination of 550-nm light over a 25 μm wide light beam. Figure 10(a) shows the cross-sectional carrier concentaion profile in a bare Si substrate, the generated carriers diffuse across the entier substrate leaving no pattern discernible. However, as shown in Fig. 10(b) the mesa array substrate utilizes the deep trench structures to halt lateral diffusion forming sharp boundaries defined by the illuminated area. Moreover, the restricted 1D diffusion allows the substrate to sustain higher carrier concentrations. Because the excess carriers in the mesa array substrate can only undergo 1D diffusion regardless of the illumination area, the carreir concentration profile can be modeled as if it were generated by a flat illumination. In the calculation, the depth of the trenches are assumed to be comparable to the substrate thickness. In practice, such a high aspect ratio strcture can be realized in Si substrates by using deap reactive ion etch (DRIE) or Bosch etching process. The surface carrier concentration profiles shown in Figs. 10(c) and 10(d) further demonstrate that when illuminated a photopattern of alphabete letter "S" on different substrates, the substrate with the mesa array structure enable to achieve high-resolution carrier distribution profiles and increase carrier concentrations. Note that the calculated carrier concentration profiles shown in Fig. 10 are captured at ~0.01 ms (a-b) and ~0.02 ms (c-d) after optical exposure starts instead of at a steady state condition. At steady state, no pattern is observalbe on the surface of the bare Si substrate due to the diffusion of the photogenerated carriers. As explained in section 3.5, the spatial resolution of THz modulation as well as modulation depth are inevitablly deteriorated by the lateral diffusion of

photogenerated carriers in the substrate. The calculated results suggest that the carrier confinement in mesa array structure provides a practial solutions to overcome the above issues. It is expected to simultaneously improve both spatial resolution of THz transmission and THz modulation depth which are essential to implement high-performance THz coded aperture imaging and manipulation of THz beam.

4. Conclusion

In conclusion, we theoretically analyzed a spectrum of physical effects on photo-induced THz wave modulation and provided the rationale for the choice of substrate material and thickness, illumination wavelength, area and power density, and THz frequency. The design guideline was suggested for the promotion of modulation depth and modulation speed which is expected to benefit the design of coded aperture imaging. While the optical properties of the substrate material play important roles in the photogeneration of excess carriers, the carrier lifetime and diffusion coefficient are the key factors governing the final modulation efficiency. These two parammeters which regulate how rapid the carriers recombine and how far they diffuse away from the excited area determine the final carrier concentration remaining in the photopatterns and therefore the THz transmission. They affect spatial and temporal resolutions of THz modulation in an opposite way. The long carrier lifetime in Ge susbtrate, for instance, promotes the generation of high excess carrier concentration and, therefore, large modulation depth. But its concurrent long diffusion length as well as slow carrier recombination degrads spatial resoltion of modulation and retards modulation speed. GaAs substrate, on the contrary, supports both high-resolution spatial modulation and high-speed tempoeral modulation. However, it requires high power light sources, such as pulsed laser, that has limited optical beam size, hindering the capability of spatial modulation. A mesa array technique was proposed to solve the issue by eliminating the lateral diffusion of carriers in Si or Ge substrate to enable low-power, large-area, high-resolution spatial modualtion of THz waves. The modulation speed will not be a concern as it is determined by the frame rate of DMD instead of the substrate material. The analysis provides the physical foundation for electron-THz wave interaction and brings insights into the design of reconfigurable THz circuits and devices.

#250139 Received 14 Sep 2015; revised 25 Nov 2015; accepted 26 Nov 2015; published 4 Dec 2015
© 2015 OSA